Journal of Structural Geology, Vol. 9, No. 4, pp. 481 to 490, 1987
Printed in Great Britain

0191-8141/87 $03.00 + 0.00
Pergamon Journals Ltd.

Extrusion and radial spreading beyond a closing channel

E. GILBERT *

Laboratoire de géologie Stratigraphique et Structurale, Université de Poitiers, 86022 Poitiers Cedex, France

and

O. MERLE

Centre Armoricain d'Etude Structurale des Socles, Université de Rennes, 35042 Rennes Cedex, France

(*Received* 12 *February* 1986; *accepted in revised form* 12 *November* 1986)

Abstract—The development of experimental models of an extruding–spreading zone beyond a closing channel is studied, and a possible natural example described. The strain pattern, folding and radial displacements within the extruding–spreading zone are analysed. Folds developed in the closing channel are either passively rotated or refolded when carried into the spreading zone. A simple theoretical model of the experiments demonstrates that the stretching lineation is radial and parallel to the displacement direction towards the base and the front of the extruding–spreading zone, but perpendicular towards the top. An intermediate domain with no stretching lineation separates the radial and concentric domains and corresponds to a transition through a uniaxial oblate ellipsoid ($K = 0$).

INTRODUCTION

LOCAL PERTURBATIONS of the strain pattern have often been described from orogenic belts (e.g. Beach 1981, Choukroune *et al.* 1986). These perturbations can be related to particular boundary conditions of major deformed zones and often represent only local strain anomalies without any major significance for crustal deformation. However, these local strain anomalies observed on strain maps (stretch and foliation trajectories) are in general poorly understood, and pose a problem. In domains of bulk horizontal shortening with lateral free boundaries, rocks can spread laterally and the strain pattern evolve progressively from the main deformed domain to the spreading domain.

An area in Ladakh (SW Himalaya) is interpreted in terms of a spreading zone in rock extruded from an area of horizontal shortening. A zone of steep fabric and vertical stretch, interpreted as due to horizontal shortening, passes continuously to a flat-lying zone where there is evidence of tangential shearing. This transition is interpreted as meaning that one boundary was free during bulk horizontal shortening and that the rocks could spread laterally. Models for such a boundary effect have been investigated experimentally and theoretically. The models provide tests for the recognition of such boundary effects in the field.

The extruding–spreading zone in our experiments is similar to that observed over the piedmont beyond a valley glacier (salt or ice) and studied by many authors (e.g. Sharp 1958, 1960, Ramberg 1964, Post 1972, Jackson 1985). The novelty of our approach is to add a lateral squeeze across the channel. Moreover, we are not concerned here with discussing the strain pattern within the channel (Hambrey 1977, Hambrey & Milnes 1977, Brun 1977, Coward 1980, Talbot & Jarvis 1984, Brun & Merle 1985) but wish to focus mainly on the extruding–spreading domain.

The purpose of this paper is therefore: (i) to study extrusion and radial spreading at lateral free boundaries during bulk horizontal shortening; (ii) to investigate the relationships between strain and displacement within such an extruding–spreading nappe; and (iii) to provide a better understanding of fold development during the extruding and spreading process.

Our model applies to superficial gravitational nappes, as frequently observed in the external domain of orogenic belts (e.g. Helvetic nappes in the central Alps). Nevertheless, in the experiments the material is squeezed out along the strike of the vertical zone and this could also feature a case in which the major displacement of the horizontally flowing nappe is along the orogenic trend.

EXPERIMENTAL MODEL

Experimental procedure

Many of the experimental techniques used were developed previously at the Experimental Tectonic Laboratory at Rennes (Cobbold & Quinquis 1980, Quinquis 1980, Hugon 1982, Brun & Merle 1985).

The apparatus corresponds to a box 18 cm long filled with silicone putty. The two long sides of the box moved towards each other so that the silicone putty was horizontally shortened. One end of the box was free and the silicone extruded and spread laterally over a rigid base when compressed (Fig. 1). Two kinds of models were

* Present address: Centre Armoricain d'Etude Structurale des Socles, Université de Rennes, 35042 Rennes Cedex, France.

SG 9:4-F

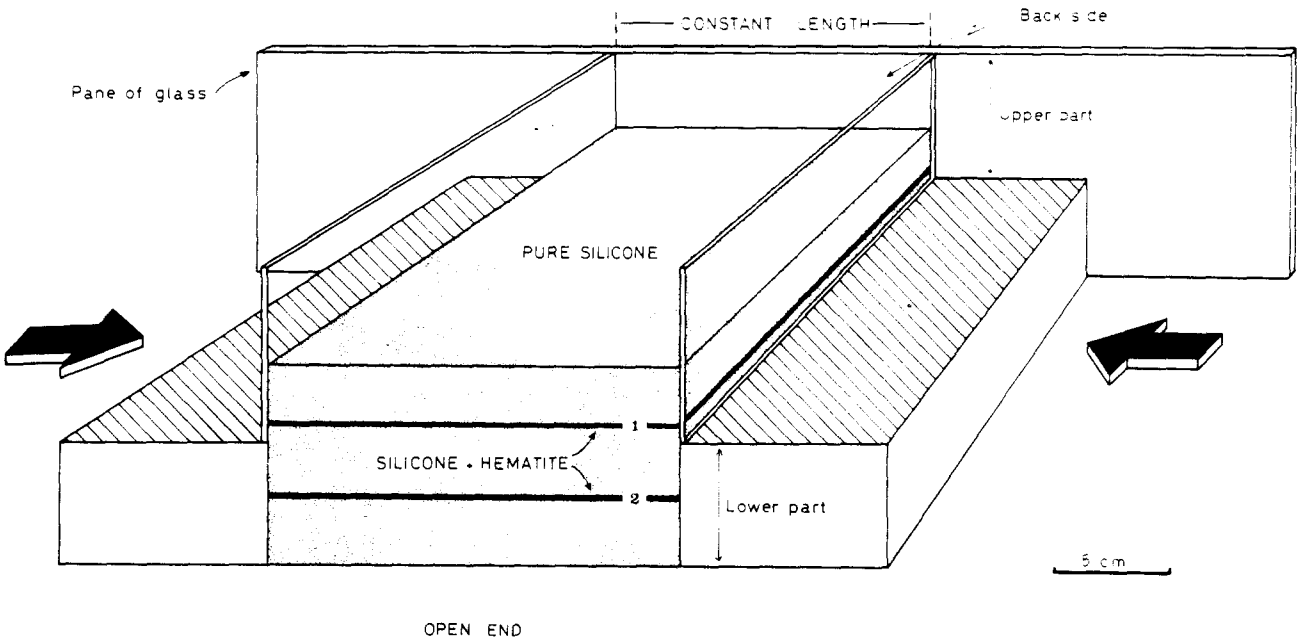

Fig. 1. Start of the model experiments of bulk horizontal shortening with a free end. Arrows show the sense of horizontal shortening and the resultant extrusion and lateral spreading from the free end.

made. In the first kind, the whole thickness of the silicone was compressed, whereas in the second only the lower part was compressed (Fig. 1). In both experiments, the silicone started in contact with a frictionless base and side walls but extruded over a base which allowed no slip along it. The side walls and base were lubricated using a solution of soap and water (Sopol, industrial detergent, BP 213, 92306 Levallois-Perret Cedex).

The viscous material in the experimental spreading zone maintained a constant vertical thickness so that the vertical axis was a direction of no strain. Practically, this is achieved by choosing a convenient ratio between the rate of extrusion and the rate of gravity-generated flow in the spreading zone. The latter rate is dependent on the thickness and viscosity of the silicone. Preliminary experiments enabled us to determine the displacement rate of each piston at about 2.25 cm h^{-1}. This balance between the extrusion and spreading processes was artificially generated in order to outline the main strain parameters within the spreading zone. The results are presented and discussed in the 'strain model' section.

The silicone putty used (Rhodorsil R. Special Gomme GSIR Rhône-Poulenc) has an almost perfectly linear dependence of stress upon strain rate, for temperatures ranging from −4 to +100°C and shear stresses less than 10 MPa. The viscosity ranges from 10^6 Pas at −40°C to 1.6×10^4 Pas at +20°C (see Dixon & Summers 1985, Weijermars 1986).

A single competent layer of Plasticine was built into the middle of model 1. The Plasticine exhibits power-law behaviour with n = 6–9 (McClay 1976). Two competent silicone layers were built into model 2 as shown in Fig. 1. The viscosity of these layers is increased by admixing finely powdered iron oxides (Fe_2O_3). The exact mixture is 49.62% of silicone and 50.38% of Fe_2O_3. The viscosity contrast between the layer and the silicone putty was then about 5 (P. R. Cobbold, personal communication).

Grids printed on the top and rear end (see Dixon & Summer 1985, Brun & Merle 1985) were photographed at regular time intervals, and the strain quantified. After both experiments, the whole apparatus was cooled down to −30°C so that serial sections could be cut and photographed without causing significant internal deformation.

Strain pattern

Strain within the closing channel. The deformed grid at the rear end and top free surface of the model allows the strain within the horizontal shortening zone to be determined. The rear end was a $\lambda_1\lambda_3$ plane ($\lambda_i = 1 + e_i$) with homogeneous horizontal shortening and vertical stretching (Fig. 2b). Such homogeneous strain was possible due to the lack of friction along the sole and sides. The channel narrowed so that λ_3 and λ_1 paralleled Z and X, respectively (see co-ordinate axes on Fig. 4).

However, as the extruding viscous material was expelled from the channel into the spreading zone λ_1 took an intermediate attitude between Y and X. Indeed the viscous fluid near the lateral free boundary was extended both vertically and horizontally. From the rear end to the free boundary of the closing channel, the strain therefore, changed from a nearly plane strain ellipsoid (Y is a direction of no strain) to a flattening type ellipsoid (with λ_3 always parallel to Z).

In this closing channel, competent layers developed folds with horizontal axes and vertical axial planes which were completely isoclinal at the end of the experiments.

Particle movement paths at the free upper surface. Photographs of the free upper surface at regular time intervals permitted mapping of particle movement paths during flow. Radial displacement was observed in every

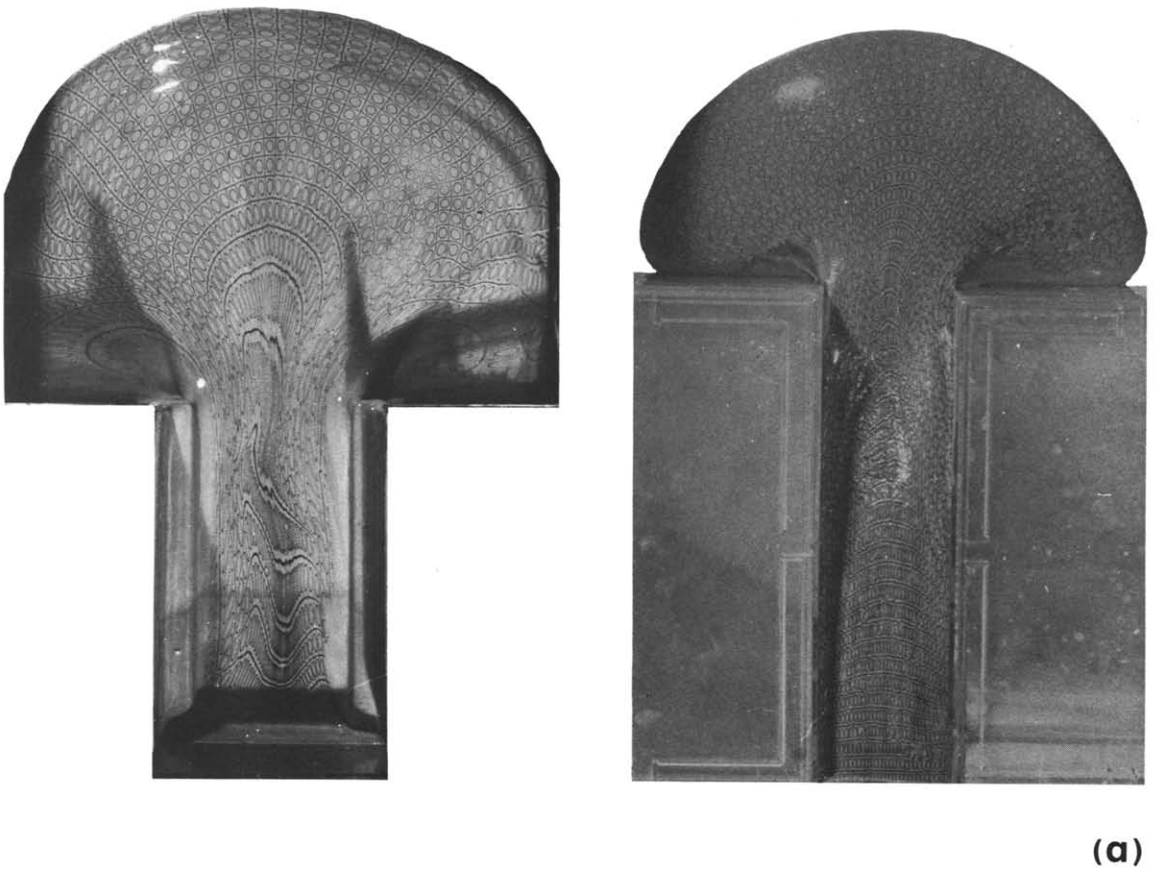

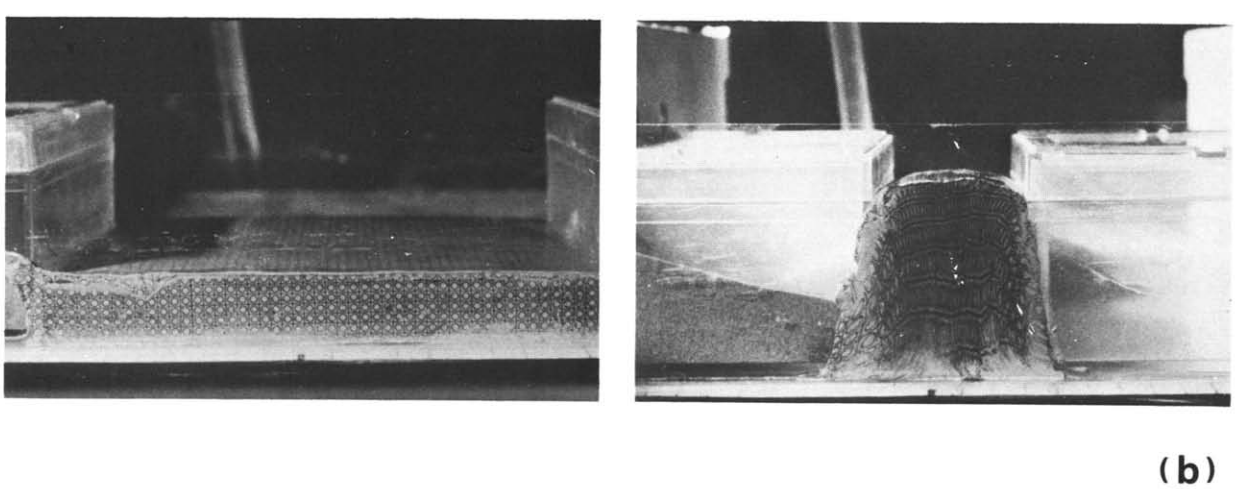

Fig. 2.(a) Plan view of the experiments. Left is the deformed grid at the free upper surface of model 1. Heterogeneous deformation in the horizontal shortening zone is due to the large wavelength and amplitude of folds developed in the competent layer. Model 2 on the right. (b) The rear end before deformation (left) and after deformation (right).

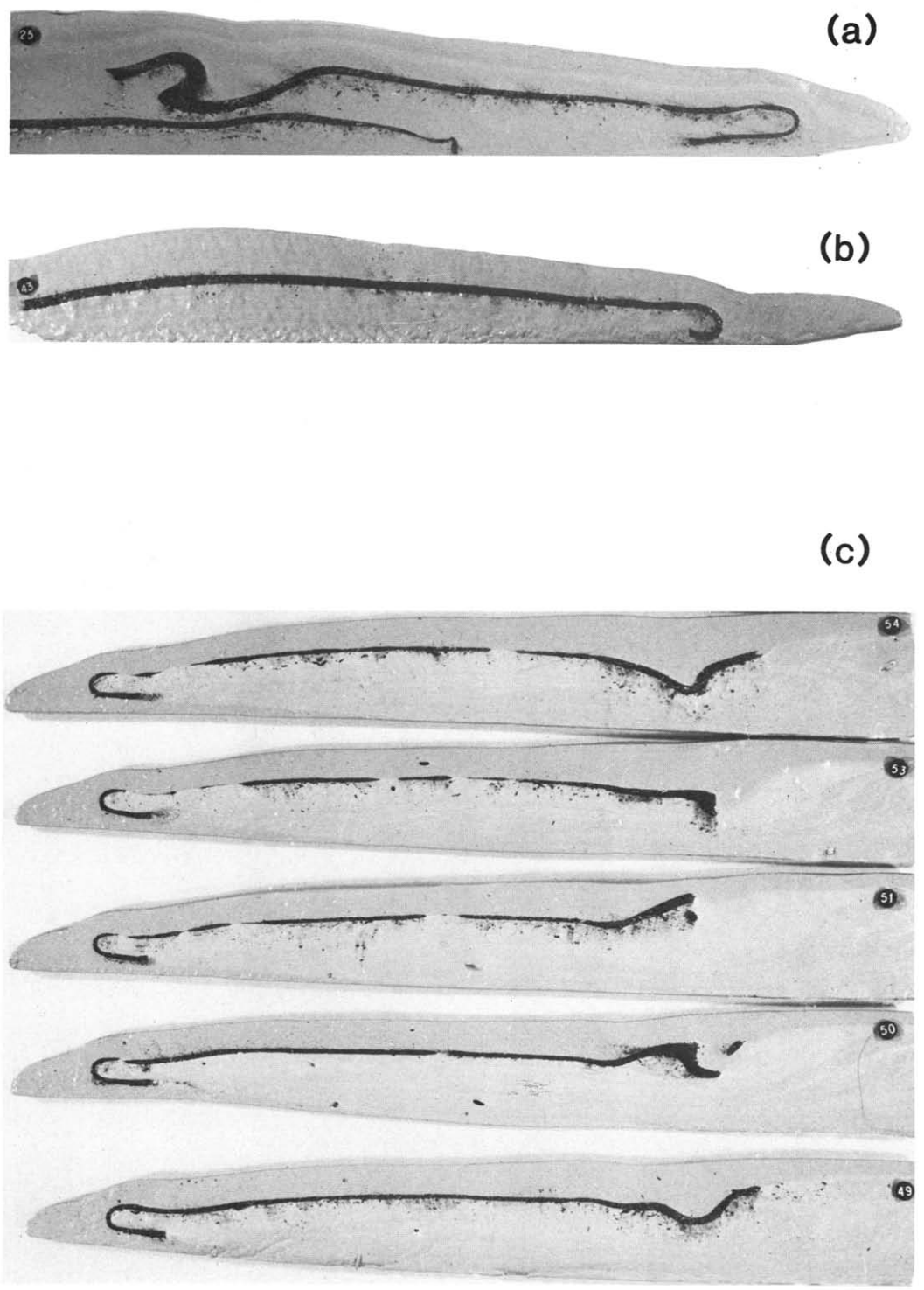

Fig. 3.(a) and (b) Cross-sections (parallel to Y) in the central part of the spreading zone. Note the frontal recumbent fold which corresponds to the rolling of the free surface at the front of the spreading zone. (a) Shows asymmetric folds developed in the model, with axes parallel to Z. (b) Is an experiment without horizontal shortening in the channel. No folds are developed in the spreading zone. (c) Serial cross-sections (parallel to Y) showing type 1 interference pattern developed in model 2. The juxtaposition of anticlines and synclines along the Z direction (observed from top to bottom) indicates dome and basin interferences.

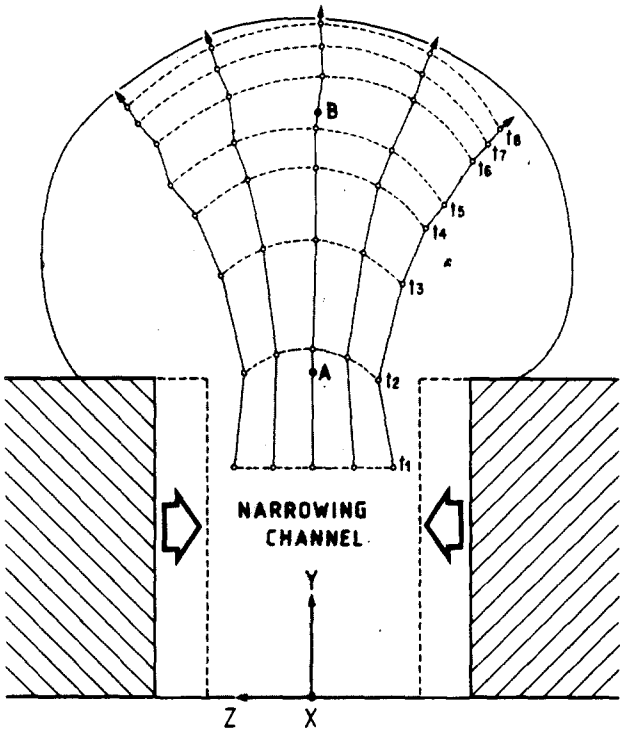

Fig. 4. Particle movement paths indicating radial displacement in the spreading zone (model 1). t_1, t_2, t_3, . . . refer to a regular time interval. (X, Y, Z, reference axes for the three-dimensional strain model). Points A and B are located on Fig. 5.

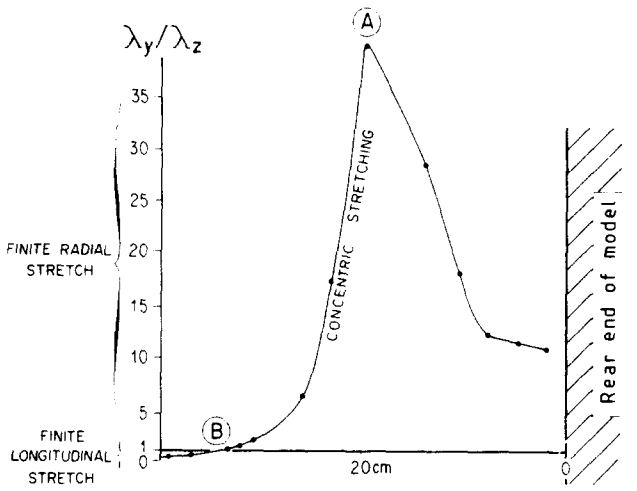

Fig. 5. Axial ratios of finite ellipses (subscripts Y and Z refer to co-ordinate axes of Fig. 4) on the free upper surface vs distance (cm) from the back side of the model along the middle line. Point A corresponds to the beginning of concentric stretching whereas point B corresponds to the change from radial to concentric or longitudinal stretch (see explanation in the text).

experiment (Fig. 4). The flow pattern is therefore radial as already observed in the piedmont of glaciers (Sharp 1960, Post 1972, Jackson 1985).

Finite strain at the top free surface. The strain at the top free surface occurred with an area change of the initial squares of the grid. This area change was especially important at the beginning of the experiments and became almost insensitive when the extruding–spreading zone was well developed (i.e. when the vertical termination of silicone at the lateral free boundary disappeared by rolling of the free surface). Area-change measurements from photographs during flow indicate that the surface increased by the same amount from back to front of the extruding–spreading zone.

The deformed grid in the extruding–spreading zone reveals two marginal wrench shearing domains near the side walls corresponding to a lateral boundary effect previously described in glaciers (Post 1972, Jackson 1985).

Photographs of the final stage of one of the experiments have been used to divide the strain in the main central part of the extruding–spreading zone into two main sub-zones (Fig. 2a and Fig. 5):

(i) a frontal (distal) sub-zone where stretching was concentric;

(ii) a back (proximal) sub-zone where stretching was radial.

The ellipses show a progressive change from radial to concentric pattern so that the two domains are separated by a line of no finite strain (point B, Fig. 5). The main characteristic of this central part is that the rectilinear lines of the initial surface grid returned to the perpendicular (or nearly so) after deformation. On the other hand, it is known that horizontal shear is zero at the free surface so that the deformed grid in the central part recorded a rotational but coaxial strain.

Incremental strain at the top free surface. The curve of finite strain (Fig. 5) may be used to describe the incremental strain during the experiment. The λ_Y/λ_Z ratio increases until point A and decreases beyond. Point A represents the location at the end of the experiment where the stretching becomes concentric. It is located about 20 cm from the rear-end of the model where lateral spreading began as the putty was extruded from the closing channel. Such a location is found again when studying the strain state of different points during time.

In other words, incremental stretching at the free upper surface is concentric in the spreading zone.

Strain model within the extruding–spreading zone. A study of the surface grid enables the relationship between stretch, stretching and displacement to be defined at the top free surface. The main result is that stretching is perpendicular to the displacement direction at the free upper surface of the extruding–spreading zone; i.e. radial displacement and concentric stretching has been recorded at the surface.

This relationship cannot be so simple within the extruding–spreading zone. It has been already noted that the horizontal shear strain must be zero at the top free surface but will exist in the interior of the model.

In order to define the relationship between strain and displacement within the extruding–spreading zone, we will attempt to define a three-dimensional strain model which takes into account all strain components during flow. A three-dimensional strain model can be mathematically expressed by a factorization of strain into simple shear (γ) and pure shear (α) components.

The pure shear component can be deduced from the strain recorded at the top free surface in the main central part of the extruding–spreading zone. The recorded coaxial strain corresponds to a shortening and extension direction parallel and perpendicular to the displacement direction, respectively (i.e. concentric stretching). On the other hand, the experimental procedure means that the vertical thickness remains almost constant (X is a direction of no strain) because of the opposing effects of the spreading process (vertical collapse) and extruding process (vertical thickening).

The deformation matrix (D_{ps}) of the pure shear component is then given by:

$$D_{ps} = \begin{vmatrix} 1 & 0 & 0 \\ 0 & \alpha^{-1} & 0 \\ 0 & 0 & \alpha \end{vmatrix} \quad \text{with } \alpha > 1,\ \alpha = 1 + eZ,\ \alpha^{-1} = 1 + eY. \tag{1}$$

A horizontal shear is superimposed onto the coaxial component within the extruding–spreading zone. It corresponds to a simple-shear component with a slide direction parallel to the displacement direction. The deformation matrix (D_{ss}) of the simple-shear component is therefore given by:

$$D_{ss} = \begin{vmatrix} 1 & 0 & 0 \\ \gamma & 1 & 0 \\ 0 & 0 & 1 \end{vmatrix}. \tag{2}$$

It must be emphasized that the pure-shear component (α) generates a concentric stretching and radial shortening whereas the simple-shear component (γ) generates a radial stretching. In our strain model, the concentric stretching (α component) is completely balanced by the radial shortening (α^{-1} component). Local proportions of α and γ therefore control whether stretching is concentric or radial.

In such a deformation process, the simple shear and pure shear are simultaneously combined so that the factorization of strain must be obtained by the strain-rate tensor rather than by the deformation gradient tensor. Rearranging Ramberg's equations (Ramberg 1975, eq. 37) and assuming steady pure-shear and simple-shear rates, the deformation gradient tensor is given by:

$$D_{ss+ps} = \begin{vmatrix} 1 & 0 & 0 \\ [\dot{\gamma}(1 - \exp(-\dot{\alpha}t))]/\dot{\alpha} & \exp(-\dot{\alpha}t) & 0 \\ 0 & 0 & \exp(\dot{\alpha}t) \end{vmatrix}, \tag{3}$$

where $\dot{\alpha}$ is the rate of change of extension and $\dot{\gamma}$ the shear strain rate. As $\alpha = \exp(\dot{\alpha}t)$ and $\gamma = \dot{\gamma}t$ then $\ln \alpha = \dot{\alpha}t$ and then $\dot{\gamma}/\dot{\alpha} = \gamma/\ln \alpha$ so that the deformation gradient tensor simplifies to:

$$D_{ss+ps} = \begin{vmatrix} 1 & 0 & 0 \\ \gamma(1 - \alpha^{-1})/\ln \alpha & \alpha^{-1} & 0 \\ 0 & 0 & \alpha \end{vmatrix}. \tag{4}$$

A similar approach was used in the study of strain patterns within nappes and thrust sheets (Coward & Kim 1981, Merle 1986).

At this stage, the strain can be computed from the Finger deformation tensor ($D.D^t$) whose eigenvalues are equal to the principal quadratic elongations and whose eigenvectors give the orientations of principal axes (see De Paor 1983).

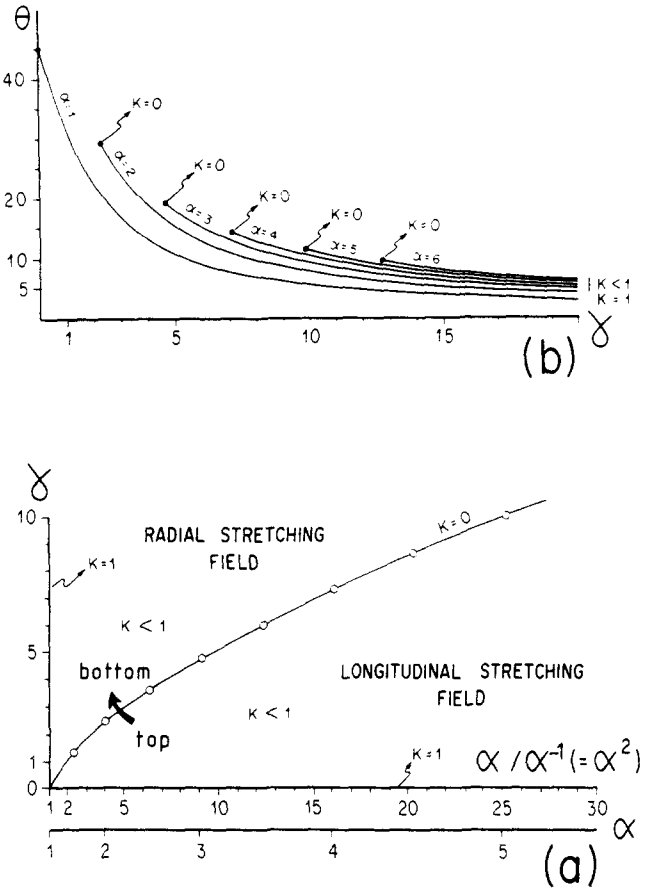

Fig. 6(a). Concentric and radial stretching as a function of simple shear (γ) and pure shear (α) components. These two domains are separated by a line which corresponds to a uniaxial oblate ellipsoid ($K = 0$). [$K = ((\lambda_1/\lambda_2) - 1)/((\lambda_2/\lambda_3) - 1)$, Flinn 1962.] The arrow indicates the strain path from top to bottom within the extruding–spreading zone (see explanation in the text). (b) Angle (θ) between the radial stretching lineation and the shear direction according to the amplitude of the simple shear component (γ) (curves of α constant value).

Results are plotted in Fig. 6(a). The line dividing the fields of radial and concentric stretching corresponds to a uniaxial oblate ellipsoid ($K = 0$). That means that a principal axis of the strain ellipsoid is constant in direction (parallel to Z) whatever the proportions of γ and α. The Z direction corresponds to the λ_1 axis in the concentric stretching domain and to the λ_2 axis in the radial stretching domain. The change between concentric and radial stretching is instantaneous without any transition. The angle between the radial stretching lineation and the horizontal can be computed from different values of the γ component (Fig. 6b). θ decreases in a way close to that for simple shear (curve $\alpha = 1$). Curves show clearly that the $\lambda_1\lambda_2$ plane (=schistosity) in the radial stretching domain is more flat-lying for higher values of the pure shearing component, α.

This mathematical approach represents the strain state at a point in the extruding–spreading zone with the assumptions previously stated. This approach allows us to define the strain pattern in the whole extruding–

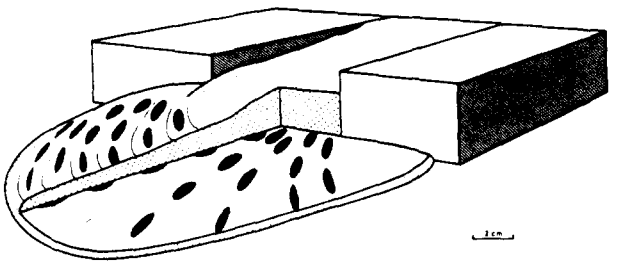

Fig. 7. Schematic representation of vertical stretch variation within the extruding–spreading zone: concentric stretching towards the top and radial stretching towards the bottom (further explanation in the text).

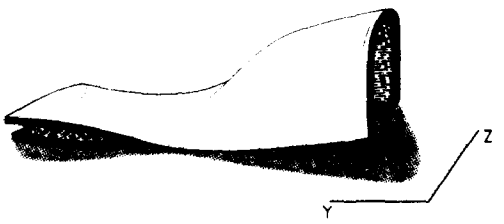

Fig. 8. Passive rotation from vertical to horizontal position of the axial plane of folds formed in the closing channel (right) when they pass into the spreading zone (left).

spreading zone. Indeed strain gradients within spreading glaciers (Hooke & Hudleston 1978, Hudleston & Hooke 1980) and spreading–gliding scale models (Brun & Merle 1985, Merle 1986) have recently been studied in detail. It is now well established that large simple shears are recorded both towards the base and the front whereas essentially pure shear is recorded towards the top. It therefore seems reasonable to assume a radial stretching lineation at the base and the front of such a spreading zone. By contrast, a concentric stretching lineation should be expected towards the top of the spreading zone (Fig. 7).

From bottom to top, radial to longitudinal stretching variation should correspond to a zone of no finite stretching lineation because of a transition characterized by a uniaxial oblate ellipsoid. Therefore, a radial stretching lineation in the field should be more usual than a longitudinal one because of the erosional effect after the emplacement of a nappe.

No strain occurred in the vertical direction in the experiments. To be a general strain model, the mathematical approach should include some vertical flattening. Nevertheless, other experiments of spreading nappes (Brun & Merle 1985) show that although vertical flattening is important at the beginning of experiments, it remains small compared to the horizontal shear component (see fig. 7 in Merle 1986). Strain measurements at the top free surface indicate also that the coaxial radial shortening is probably much more important than the vertical flattening (compare Fig. 3a & b).

This strongly suggests that the strain model developed in this paper could apply to natural extruding–spreading nappes whether they flatten vertically or not. Such a deformation sequence from top to bottom (stretching perpendicular to the displacement at the top and parallel at the base, with an intermediate zone of no stretching) has been described in the Helvetic nappes by Ramsay (1981, p. 302), so this strain model is likely to be found in superficial gravity tectonics. We believe that our strain model provides a possible explanation for vertical stretch variations within the Helvetic nappes.

Folding

Folds as a result of flow in a channel have been extensively studied for over 20 years (Ramberg 1964, Post & La Chapelle 1971, Post 1972, Hudleston 1976, 1977, Talbot 1979, 1981, Merle & Brun 1982). Fold limbs defined by boundary-parallel shear zones due to strain gradients develop with axial surfaces parallel to all rigid boundaries. Flow is subparallel to the fold axial trace. Such folds can be observed on the top free surface of model 1 (Fig. 2a, left). They resulted from differential horizontal flow linked to large amplitude folding of the plasticine layer within the model and did not develop at the upper free surface of model 2 (Fig. 2a, right). The distal spreading front rolls over the frictional base resulting in a frontal recumbent fold (Fig. 3). This rolling process is purely kinematic and also develops in spreading models without any viscosity contrast between the layering (Brun and Merle 1985, Merle 1986).

In this section we describe folding of competent layers in order to provide some insight into fold development within an extruding–spreading zone. This concerns: (i) the deformation of folds developed in the closing channel when carried into the extruding–spreading zone (model 1); and (ii) the fold development within the extruding–spreading zone (model 2).

Buckling of the Plasticine layer (model 1). In model 1, the horizontal Plasticine layer developed buckles with vertical axial planes and horizontal axes in the closing channel. These buckles passed into the extruding–spreading zone where the axial plane passively rotated from vertical to horizontal and the folds axes curved down with them (Fig. 8).

Folding within an extruding–spreading zone (model 2). Only the lower part of the silicone was compressed in model 2 so that the upper layer was not horizontally shortened (Fig. 1). The lower competent layer was buckled in the horizontally shortened zone as previously described in model 1. Where the buckled layer passed into the spreading zone, it was folded again on horizontal axes perpendicular to those developed in the horizontally shortened zone. Type 1 interference patterns (dome and basin, see Ramsay 1967, p. 522) are observed from different cross-sections of the spreading zone at the end of the experiment (Fig. 3c).

The upper competent layer developed a fold-couple only in the extruding–spreading zone (Fig. 3a). The asymmetry of these folds is consistent with the bulk shear within the extruding–spreading zone. In order to clarify parameters controlling fold development, an additional experiment was performed where the silicone was allowed to spread laterally without closing the channel. No folds developed during the steady flow in this last

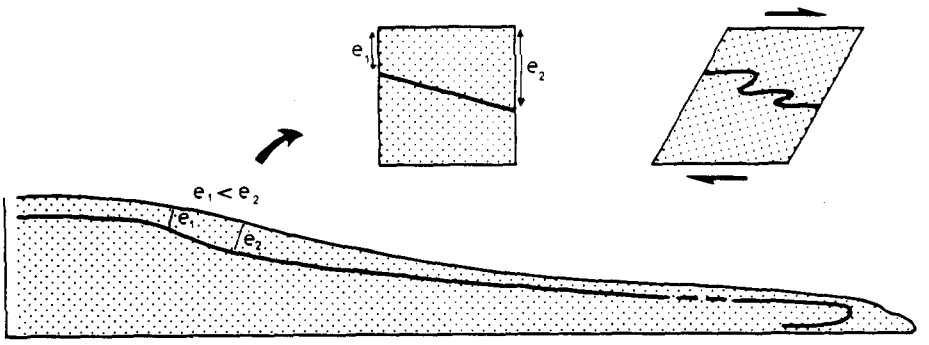

Fig. 9. Differential flow rates between the competent layer and the silicone result in a change in the thickness of silicone above the competent layer (model 2). The competent layer is folded as a result of simple shear in a similar manner to the experiments of Cobbold & Quinquis (1980, model 1) and Hugon (1982) (see also Hudleston 1977).

experiment (Fig. 3b). This shows that lateral squeeze across the channel is necessary for folds to develop in our experiments. The kinematic process of folding is schematically represented in Fig. 9. The viscosity contrast between the competent layers and silicone matrix induced a differential flow rate that caused a change in the thickness of silicone above the competent layer. The shearing due to departure from steady-state flow induced by changes in boundary conditions accounts for the internal folds described by Hudleston (1976, 1977) and Talbot (1979).

FIELD EXAMPLE

The Mulbeck Chu Nappe in Ladakh (NW Himalaya)

The Mulbeck Chu Nappe is developed in calcareous deposits of the Indian platform (Triassic to Maestrichtian). It is structurally located above the 'Dalle du Tibet' and limited to the north by the Indus Suture Zone (Fuchs 1982, 1986, Baud *et al.* 1984, Colchen *et al.* 1986). The strain and main deformational structures have been studied in some detail (Gilbert 1986) and will be pub-

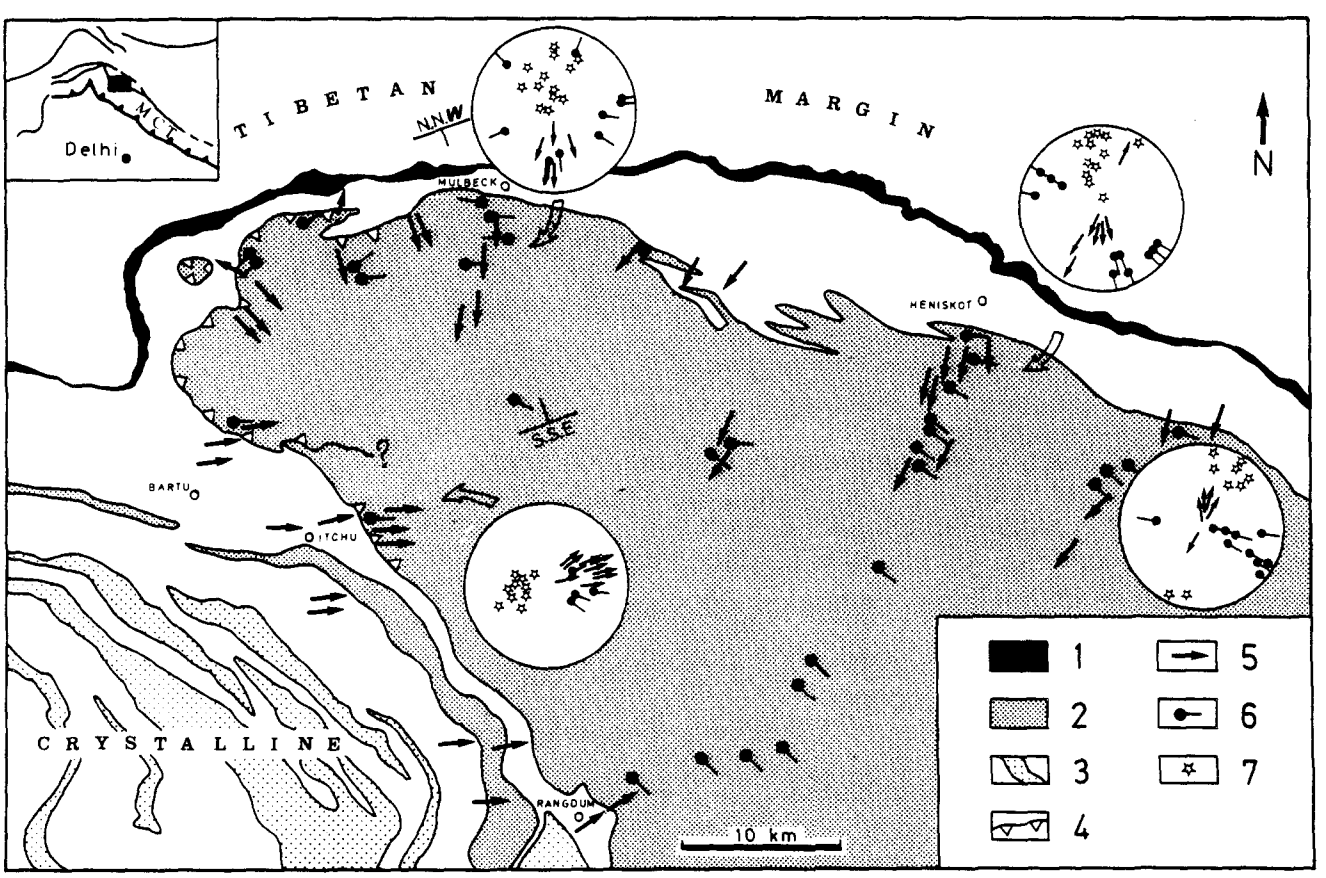

Fig. 10. Structural map of the western Zanskar of the NW Himalayas: 1: ophiolitic melange (Indus Suture Zone); 2: Mesozoic and Cenozoic cover of the Indian margin; 3: granitoids and crystalline rocks of the High Himalaya; 4: thrust; 5: stretching lineation; 6: fold axes; 7: poles of axial planes. The cross-section in Fig. 11 is shown by the positions labelled NNW and SSE.

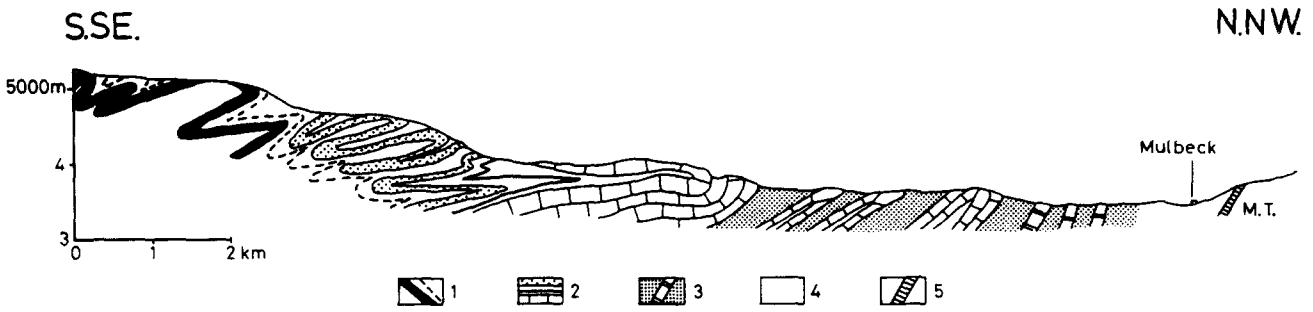

Fig. 11. Geological cross-section along the Mulbeck Chu river (see location on the Fig. 10). 1: Lilang formation (Triassic); 2: Kioto formation (Upper Trias-Lias); 3: Fatu-la formation (Cretaceous); 4: Lamayuru flysch; 5: ophiolitic melange (Indus Suture Zone); M.T.: Tibetan Margin.

lished elsewhere. Our purpose is to present here the main features of the Mulbeck Chu Nappe as an example of extrusion and radial spreading at a lateral free boundary during bulk horizontal shortening.

The studied area can be divided into three main zones (Fig. 10).

(1) The northeastern part (south of Heniskot) corresponds to a horizontal shortening zone with vertical schistosity and stretching lineation. Folds are similar in style with vertical axial planes and horizontal axes (Fig. 10). The strain observed in this zone is similar to that observed in the closing channel of our models (Fig. 2b; deformed grid).

(2) The western part corresponds to a spreading zone with a radial stretching lineation systematically perpendicular to the fold axes (Fig. 10). The strain increases from top to bottom, as shown by concentric folds at the top and similar folds at the bottom. This is associated with the axial planes rotating from 45° to horizontal (Fig. 11 and model 2).

A mylonitic zone associated with a very strong shear component in the displacement direction is located at the base of the nappe. At the front of the nappe, the stratigraphic units are inverted (Jurassic over Cretaceous). This inversion could be interpreted as resulting from the rolling process observed at the front of our model (Fig. 3).

(3) A transitional zone shows a rapid variation of fold axis plunge (from horizontal to 70° and back to horizontal) associated with the change from vertical to horizontal axial plane in the spreading zone. This spatial variation is similar to that observed in model 1 (Fig. 8).

The concentric stretching domain observed in the experiment towards the top of the spreading zone is not observed in the field example. This absence is thought to be the result of erosion of the top free surface of the nappe.

CONCLUSIONS

The main conclusions of this study of rocks and their analogues extruding radially over a piedmont from a closing channel are as follows.

(1) Radial displacement is observed in the extruding–spreading zone.

(2) A strain model within the extruding–spreading zone has been deduced from the strain observed at the free upper surface during experiments. Stretching would be parallel to the displacement (i.e. radial) at the base and at the front of the model, but perpendicular to the displacement at the top. An intermediate zone of no stretching lineation ($\lambda_1 = \lambda_2$, $K = 0$) separates these two domains.

(3) If we except the frontal rolling zone, the lateral squeeze across the channel seems to be a necessary condition for fold development within the extruding–spreading zone in our experiments.

(4) Axial planes of folds passively rotate from vertical in the channel to horizontal in the extruding–spreading zone.

(5) Interference patterns are observed between folds which developed in the closing channel and were refolded in the extruding–spreading zone.

(6) Folds developed into the extruding–spreading zone are non-cylindrical and strongly asymmetric, if not sheath-like.

Acknowledgements—Thanks are especially due to P. R. Cobbold for critically reading the manuscript. D. Gapais is gratefully acknowledged for useful comments during the development of this work. We are also indebted to C. J. Talbot for his careful review of the manuscript and his suggestions for improvement.

REFERENCES

Baud, A., Gaetani, M., Garzanti, E., Fois, E., Nicora, A. & Tintori, A. 1984. Geological observations in southeastern Zanskar and adjacent Lahul area (northwestern Himalaya). *Eclog. geol. Helv.* **77**, 171–197.

Beach, A. 1981. Some observations on the development of thrust faults in the Ultradauphinois zone, French Alps. In: *Thrust and Nappe Tectonics* (edited by McClay, K. & Price, N. J.). *Spec. Publs geol. Soc. Lond.* **9**, 329–334.

Brun, J. P. 1977. Cumulative strain and boundary effects in the gravity flow of a viscous slab. *Tectonophysics* **41**, T7–T14.

Brun, J. P. & Merle, O. 1985. Strain patterns in models of spreading-gliding nappes. *Tectonics* **4**, 705–719.

Choukroune, P., Ballevre, M., Cobbold, P. R., Gauthier, Y., Merle, O. & Vuichard, J. P. 1986. Deformation and motion in the Western Alpine Arc. *Tectonics* **5**, 215–226.

Cobbold, P. & Quinquis, H. 1980. Development of sheath folds in shear regimes. *J. Struct. Geol.* **2**, 119–126.

Colchen, M., Mascle, G. & Van Haver, Th. 1986. Some aspects of collision tectonics in the Indus Suture Zone, Ladakh. In: *Collision Tectonics. Spec. Publs geol. Soc. Lond.* **19**, 173–184.

Coward, M. P. 1980. The analysis of flow profiles in a basaltic dyke using strained vesicles. *J. geol. Soc. Lond.* **137**, 605–615.

Coward, M. P. & Kim, J. H. 1981. Strain within thrust sheets. In: *Thrust and Nappe Tectonics* (edited by McClay, K. & Price, N. J.). *Spec. Publs geol. Soc. Lond.* **9**, 275–292.

De Paor, D. G. 1983. Orthographic analysis of geological structures. Deformation theory. *J. Struct. Geol.* **5**, 255–277.

Dixon, J. M. & Summers, J. M. 1985. Recent development in centrifuge modelling of tectonic processes: equipment, model construction techniques and rheology of model materials. *J. Struct. Geol.* **7**, 83–102.

Flinn, D. 1962. On folding during three-dimensional progressive deformation. *Q. Jl geol. Soc. Lond.* **118**, 385–434.

Fuchs, G. 1982. The geology of Western Ladakh. *Jber. geol. Bundesanst.* **125**, 1–50.

Fuchs, G. 1986. The geology of the Markha-Khurnak region in Ladakh (India). *Jber. geol. Bundesanst.* **128**, 403–437.

Gilbert, E. 1986. Evolution structurale d'une chaîne de collision: Structures et deformation dans le Nord de la plaque Indienne en Himalaya du Ladakh. Thesis, Université de Poitiers.

Hambrey, M. J. 1977. Foliation, minor folds and strain in glacier ice. *Tectonophysics* **39**, 397–416.

Hambrey, M. J. & Milnes, A. G. 1977. Structural geology of an Alpine glacier (Griesgletscher, Valais, Switzerland). *Eclog. geol. Helv.* **70**, 667–684.

Hooke, R. B. & Hudleston, P. J. 1980. Origin of foliation in glaciers. *J. Glaciol* **20**, 285–299.

Hudleston, P. J. 1976. Recumbent folding in the base of the Barnes Ice Cap, Baffin Island, Northwest territories, Canada. *Bull. geol. Soc. Am.* **87**, 1684–1692.

Hudleston, P. J. 1977. Similar folds, recumbent folds and gravity tectonics in ice and rocks. *J. Geol.* **85**, 113–122.

Hudleston, P. J. & Hooke, R. B. 1980. Cumulative deformation in the Barnes Ice Cap and implications for the development of foliation. In: *Analytical Studies in Structural Geology* (edited by Schwerdtner, W. M., Hudleston, P. J. & Dixon, J. M.). *Tectonophysics* **66**, 127–146.

Hugon, H. 1982. Structure et déformation du massif de Rocroi (Ardennes), approche géométrique quantitative et expérimentale. Thèse 3e Cycle, University of Rennes.

Jackson, M. P. A. 1985. Natural strain in diapiric and glacial rock salt, with emphasis on Oakwood Dome, East Texas. Report of investigations No. 143, Bureau of Economic Geology, Austin, Texas.

McClay, K. R. 1976. The rheology of plasticine. *Tectonophysics* **33**, T7–T15.

Merle, O. 1986. Patterns of stretch trajectories and strain rates within spreading–gliding nappes. *Tectonophysics* **124**, 211–222.

Merle, O. & Brun, J. P. 1982. Superimposed fabrics and progressive deformation during the emplacement of the Parpaillon Nappe (Helminthoïd flysch, French Alps). *Int. Conf. on Planar Fabrics of Deformed Rocks, Zurich. Abstr.*

Post, A. 1972. Periodic surge origin of folded medial moraines on Bering piedmont glacier, Alaska. *J. Glaciol.* **11**, 219–226.

Post, A. & La Chapelle, E. R. 1971. *Glacier Ice.* University of Washington Press, Seattle, Washington, U.S.A.

Quinquis, H. 1980. Schistes bleus et déformation progressive, l'exemple de l'Ile de Groix (Massif Armoricain). Thèse 3e Cycle, University of Rennes.

Ramberg, H. 1964. Note on model studies of folding of moraines in piedmont glaciers. *J. Glaciol.* **5**, 207–218.

Ramberg, H. 1975. Particle paths, displacement and progressive strain applicable to rocks. *Tectonophysics* **28**, 1–37.

Ramsay, J. G. 1967. *Folding and Fracturing of Rocks.* McGraw-Hill, New York.

Ramsay, J. G. 1981. Tectonics of the Helvetic nappes. In: *Thrust and Nappe Tectonics* (edited by McClay, K. & Price, N. J.). *Spec. Publs geol. Soc. Lond.* **9**, 293–309.

Sharp, R. P. 1958. Malaspina glacier, Alaska. *Bull. geol. Soc. Am.* **69**, 617–646.

Sharp, R. P. 1960. *Glaciers.* University of Oregon Press, Eugene, Oregon, U.S.A.

Talbot, C. J. 1979. Fold trains in a glacier of salt in southern Iran. *J. Struct. Geol.* **1**, 5–18.

Talbot, C. J. 1981. Sliding and other deformation mechanisms in a glacier of salt. S. Iran. In: *Thrust and Nappe Tectonics* (edited by McClay, K. & Price, N. J.). *Spec. Publs geol. Soc. Lond.* **9**, 173–183.

Talbot, C. J. & Jarvis, M. J. 1984. Age, budget and dynamics of an active salt extrusion in Iran. *J. Struct. Geol.* **6**, 521–533.

Weijermars, R. 1986. Flow behaviour and physical chemistry of bouncing putties and related polymers in view of tectonic laboratory applications. *Tectonophysics* **124**, 325–358.